CHEMISTRY
A EUROPEAN JOURNAL

DOI: 10.1002/chem.201102607

Smectic-Layer Alignments of Surface-Modified Gold Nanoparticles in the Nanocomposite Induced by a Hydrogen-Bonded Bent-Core Liquid Crystalline Host under Electric Fields

Wei-Hong Chen,[a] Yi-Ting Chang,[a] Jey-Jau Lee,[b] Wei-Tsung Chuang,[b] and Hong-Cheu Lin*[a]

There has been great interest recently in the fabrication of highly ordered metal nanoparticle (NP) assemblies.[1] Large scale periodical arrangements of NPs are fascinating systems for the development of nanostructural materials exhibiting new electronic,[2] magnetic,[3] optical,[4] and photonic properties.[5] Many examples of the application of templates have appeared for the generation of ordered assemblies of NPs, by using, for example, surface-modified polymers,[6] self-assembled monolayers,[7] lipid films,[8] and DNA.[9] In addition, the self-organization behavior of gold NPs surface-modified with rod-like,[10] bent-core,[11] and discotic[12] liquid crystal (LC) surfactants has been reported. Moreover, several strategies have been proposed to template arrays of NPs by using block copolymer systems, in which the spatial arrangements are directed through self-assembly of the block copolymers.[13] LC materials possessing a variety of mesomorphic structures can be aligned in a straightforward manner through the application of electric fields,[14] magnetic fields,[15] and polymer networks.[16] The self-organization of LC molecules is determined by the characteristic arrangements of the mesophasic types, including the nematic, cholesteric, smectic, and columnar phases.

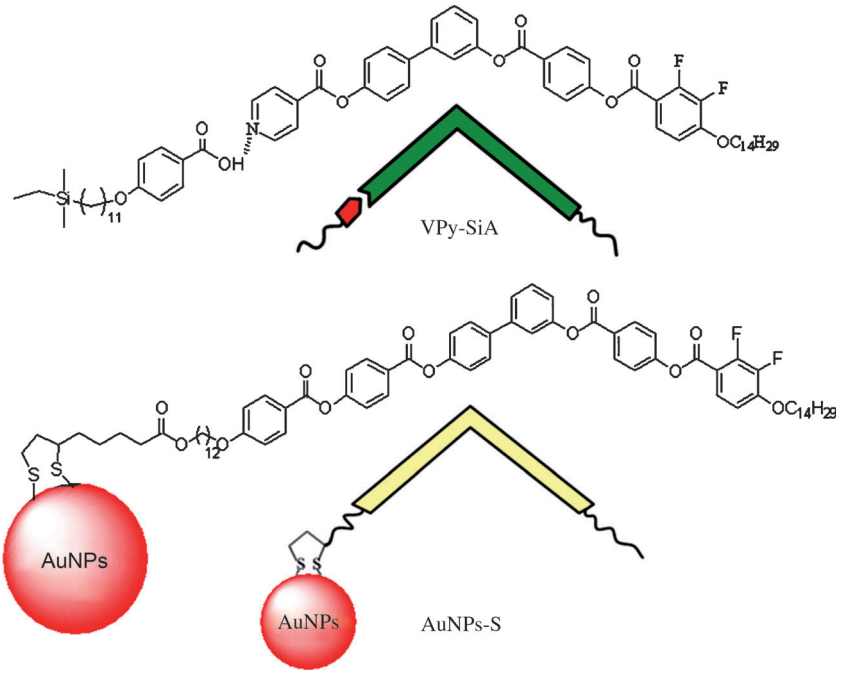

Scheme 1. Chemical structures of the hydrogen-bonded bent-core LC host VPy-SiA (containing the hydrogen bond acceptor VPy and the hydrogen bond donor SiA) and the surface-modified gold NPs AuNPs-S presenting the covalently bonded bent-core surfactant S.

Herein, we describe the synthesis of the novel hydrogen-bonded bent-core LC host VPy-SiA (bearing a flexible carbosilane chain) and the gold nanocomposite (VPy-SiA/AuNPs-S) by adding 5 wt% the surface-modified gold NPs (AuNPs-S) to the self-assembled LC host (VPy-SiA; Scheme 1). We developed a novel in situ technique for alignment of the nanocomposite VIPy-SiA/AuNPs-S under (DC/AC) electric fields, and examined the orientation behavior of the smectic layer structures using two-dimensional X-ray diffraction patterns and frozen transmission electron microscopy (FTEM). To the best of our knowledge, no previous reports have described the ordered layer arrangements of NPs in a nanocomposite—induced by compatibility of the NPs in the phase of the LC hosts—that could then be further aligned under electric fields.

[a] W.-H. Chen, Y.-T. Chang, Prof. H.-C. Lin
Department of Materials Science and Engineering
National Chiao Tung University, Hsinchu 300 (Taiwan)
Fax: (+8863) 5724727
E-mail: linhc@cc.nctu.edu.tw

[b] J.-J. Lee, W.-T. Chuang
National Synchrotron Radiation Research Center
Hsinchu, 30076 (Taiwan)

Supporting information for this article is available on the WWW under http://dx.doi.org/10.1002/chem.201102607.

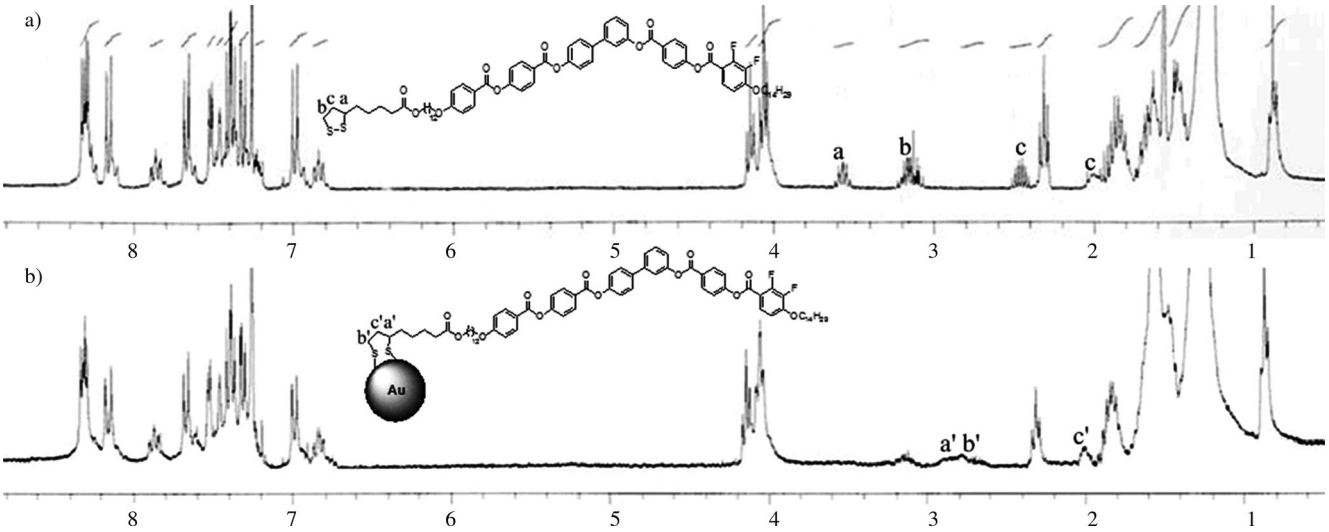

Figure 1. ^{1}H NMR spectra of: a) surfactant S (signals marked a, b, and c correspond to specific protons of the disulfide unit), and b) the gold NPs AuNPs-S (signals marked a', b', and c' represent the corresponding protons after ring opening and attachment of the disulfide unit to the gold NPs).

Figure 1 presents the ^{1}H NMR spectra of the covalently bonded bent-core surfactant S and the surface modified gold NPs, AuNPs-S. The broad signals in the ^{1}H NMR spectrum of AuNPs-S were caused by the dipolar spin relaxation of the surfactant S units on the surface of the gold NPs.[17] The up-field shift and broadness of the methine proton (proton a') of the attached surfactant S unit were probably due to restricted ligand rotation in the proximity of the gold surface. Two new signals (protons b' and c') appeared for the disulfide units of AuNPs-S after ring opening and attachment of disulfides to the gold NPs. The TEM image in Figure S1 in the Supporting Information indicates that the surface stabilized gold NPs (AuNPs-S) had an average diameter of (2.5 ± 0.8) nm. The inflammable part of the ligands was 48% AuNPs-S and a 9 wt% char yield of S ($>800\,^\circ$C; Figure S2 in the Supporting Information). The number of Au atoms in one cluster of AuNPs-S was calculated with Equation (1), where n is the number of atoms per cluster, R is the NP radius ((2.5 ± 0.8) nm, TEM), and ν_g is the molar volume of Au ($\nu_g=10.2\ \mathrm{cm^3\,mol^{-1}}$). The number of ligands in one cluster of AuNPs-S was estimated by using Equation (2), where N is the number of ligands per cluster, A_w is the atomic weight of Au, M_w is the molecular weight of ligand S [Eq. (2) is a rearrangement of the equation, wt% of ligand $=(N\times M_w)/(N\times M_w+n\times A_w]$:

$$n\mathrm{Au}=\frac{4\pi R^3}{3\nu_g} \tag{1}$$

$$N=\frac{n\times A_w\times \mathrm{wt\,\%\ of\ ligand}}{M_w\times \mathrm{wt\,\%\ of\ Au}} \tag{2}$$

Accordingly, we could roughly calculate[18] an average of 481 gold atoms and 99 ligand molecules on the surface-modified gold NPs AuNPs-S by combining the TGA data with the average particle size obtained from the TEM image.

Table 1. Mesomorphic properties (phase transition temperatures, enthalpies) of the hydrogen-bonded bent-core complex VPy-SiA and its gold nanocomposite VPy-SiA/AuNPs-S incorporating 5 wt% surface-modified gold NPs (AuNPs-S).[a]

Complex	Phase transition temperature [°C] and enthalpy [J g^{-1}]
VPy-SiA	Cr $\underset{91.7\ [14.3]}{\overset{110.3\ [16.3]}{\rightleftharpoons}}$ $SmCP_A$ $\underset{126.6\ [23.6]}{\overset{130.2\ [23.6]}{\rightleftharpoons}}$ Iso
VPy-SiA/AuNPs-S (5 wt%)	Cr $\underset{87.0\ [12.2]}{\overset{108.7\ [14.2]}{\rightleftharpoons}}$ $SmCP_F$ $\underset{125.3\ [21.8]}{\overset{129.1\ [23.0]}{\rightleftharpoons}}$ Iso

[a] Iso: isotropic state; Cr: crystalline state; $SmCP_A$: "nonclassical" AF switching polar smectic phase; $SmCP_F$: FE switching polar smectic phase. The phase transitions were measured by DSC at the second heating and cooling scans with a rate of 5 °C min^{-1}.

Table 1 lists the mesomorphic properties (phase transition temperatures, enthalpies) of the hydrogen-bonded bent-core complex VPy-SiA and its gold nanocomposite VPy-SiA/AuNPs-S (5 wt%). Relative to the hydrogen bonded complex VPy-SiA, we observed broader mesophasic ranges for the nanocomposite VPy-SiA/AuNPs-S (5 wt%), which exhibited a polar smectic (B2 or SmCP) phase[19] during both the heating and cooling processes (Figure S3 in the Supporting Information displays the fan-like textures of these samples).

The results of the switching current experiments (Figure 2a and b) at a temperature (T) of 110 °C reveal a single well-resolved repolarization current peak in each half period of the applied triangular wave at V_{pp} values of 300 and 150 V (both reaching saturated polarization) for the complex VPy-SiA and the nanocomposite VPy-SiA/AuNPs-S (5 wt%), respectively. The modified triangular wave method can also be used to understand the actual switching current behavior. To determine the polarity of the SmCP

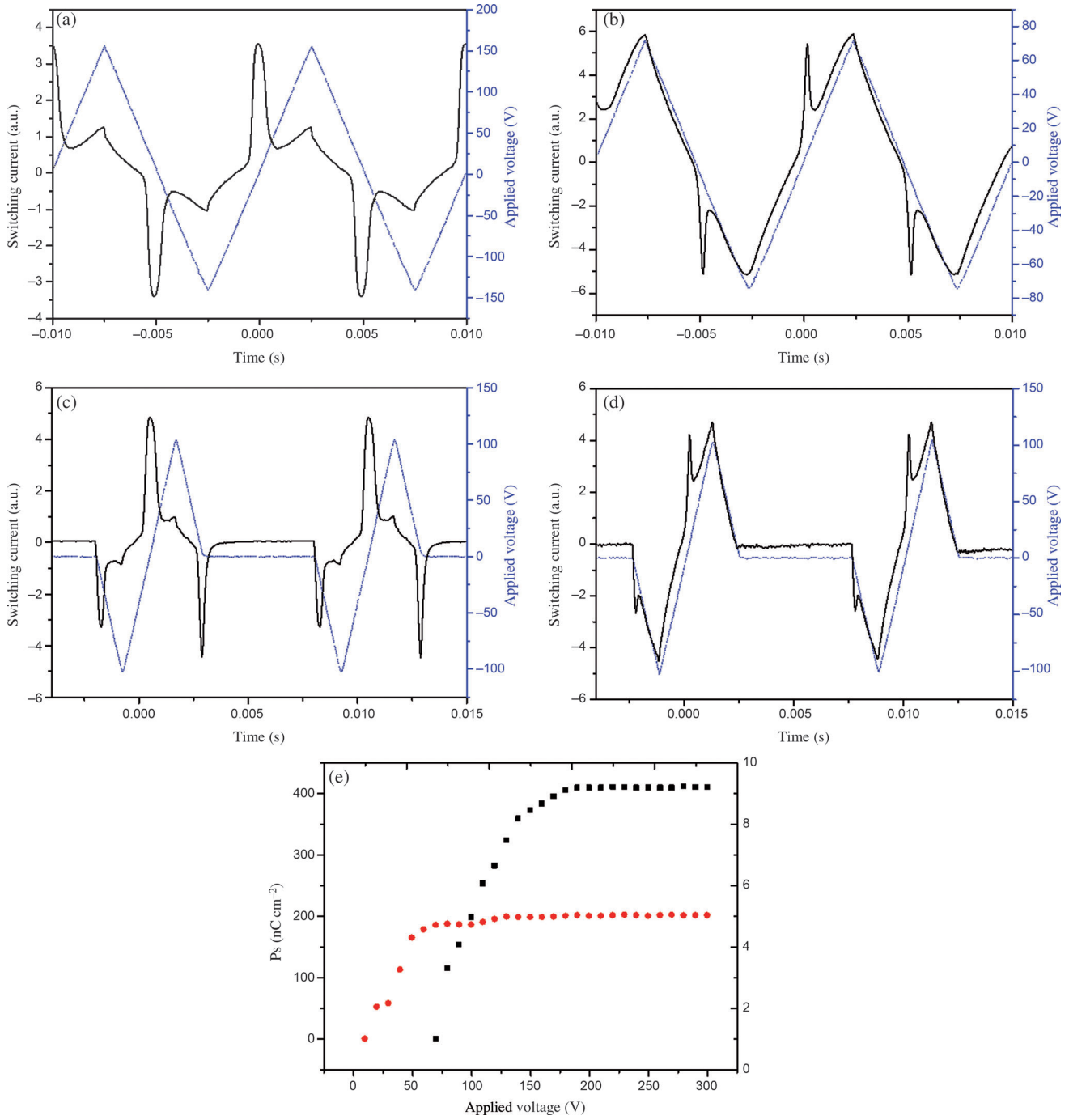

Figure 2. Switching current responses at 110 °C by using the triangular wave method (100 Hz) for: a) the hydrogen-bonded complex VPy-SiA (V_{pp}= 300 V), and b) the nanocomposite VPy-SiA/AuNPs-S (5 wt %; V_{pp}=150 V); and the modified triangular wave method for: c) VPy-SiA (V_{pp}=200 V), and d) VPy-SiA/AuNPs-S (5 wt %; V_{pp}=200 V). e) Values of P_s plotted with respect to the applied voltages for VPy-SiA (■) and its nanocomposite VPy-SiA/AuNPs-S (5 wt %; ●).

phase in the complex VPy-SiA and the composite VPy-SiA/AuNPs-S (5 wt %), the switching current phenomena of the modified triangular wave (f=100 Hz) clearly revealed "non-classical" antiferroelectric (AF) switching[20] with two peaks for the $SmCP_{A'}$ phase and ferroelectric (F) switching with one peak for the $SmCP_F$ phase. Hence, the complex VPy-SiA exhibited the $SmCP_{A'}$ phase, as verified by the fact that the current response was divided into two repolarization peaks under the modified triangular wave at a single pulsed triangular wave with a V_{pp} value of 200 V (Figure 2c provides one example).

In contrast, Figure 2d reveals that only one repolarization peak has the $SmCP_F$ phase under the modified triangular wave when supplying the nanocomposite VPy-SiA/AuNPs-S

(5 wt %) with a single pulsed triangular wave with a V_{pp} value of 200 V. As illustrated in Figures S4 and S5 in the Supporting Information, rotations of the circular domains occurred in the hydrogen-bonded complex VPy-SiA. Figure 2e displays the P_s values with respect to the applied voltages. The values of saturated P_s of the SmCP phases ($SmCP_F$ and $SmCP_A$) were all reached at specific saturated voltages (V_s, where it reached the saturated P_s), with the values of saturated P_s and V_s both correlated to the content of AuNPs-S. The value of saturated P_s decreased from 410 to 190 $nC\,cm^{-2}$ and the value of V_s decreased from approximately 180 to 70 V upon increasing the gold NP concentration from 0 to 5 wt %. Therefore, doping with the gold NPs decreased the value of P_s of the nanocomposite VPy-SiA/AuNPs-S as a result of the dilution (and/or dispersion) effect of the polar arrangement, but the surface modified gold NPs also reduced the operating voltage of the device.

To understand molecular stacking behavior, alignment techniques can be performed while applying external electric or magnetic fields. Here, we recorded in situ electric field XRD and FTEM data by using the same apparatus (Figure S6 in the Supporting Information). Figure S7 in the Supporting Information presents 1D XRD profiles of the hydrogen bonded complex VPy-SiA and the nanocomposite VPy-SiA/AuNPs-S (5 wt %). Upon increasing the content of AuNPs-S from 0 to 5 wt %, the value of d_1 increased proportionally from 5.34 to 5.5 nm, due to insertion of the surface-modified AuNPs-S into the smectic layer of VPy-SiA in the nanocomposite VPy-SiA/AuNPs-S.

Furthermore, the hydrogen-bonded complex and all of the nanocomposite exhibited comparable wide-angle diffuse halos, corresponding to d spacings of 0.44 nm; this indicates that similar liquid-like, in-plane orders with analogous average intermolecular distances were prevalent within the smectic layers of these studied compounds. To evaluate the detailed orientational relationship between the layer structures (small-angle region) and the intermolecular packing (wide-angle region), we recorded the 2D diffraction patterns (at 110 °C during the cooling process) of the complex VPy-SiA and the nanocomposite VPy-SiA/AuNPs-S (5 wt %), respectively. Based on the results of the small-angle arcs (Figure 3a and c), we deduced that the smectic layer normal (small-angle region), which is also parallel to the equator, was perpendicular to the direction of the electric fields. Figure 3b and d reveal that the direction of the smectic layer was aligned along the equator direction, with a highly ordered smectic structure.

We then used FTEM to evaluate the distribution of the gold NPs (AuNPs-S) and their self-assembly behavior under DC/AC electric fields in the nanocomposite VPy-SiA/AuNPs-S. The electrode setup (Figure S6 in the Supporting Information) for these FTEM experiments was the same as that used for the in situ XRD diffraction experiments. Figure 4 displays FTEM images of the quenched LC structures of the nanocomposite VPy-SiA/AuNPs-S (5 wt %), which had been quenched through rapid immersion of the LC phase in liquid N_2 and removed from the electrodes (in the presence and absence of DC/AC electric fields). The gold NPs (AuNPs-S) were randomly distributed in the nanocomposite VPy-SiA/AuNPs-S (5 wt %) in the absence of an

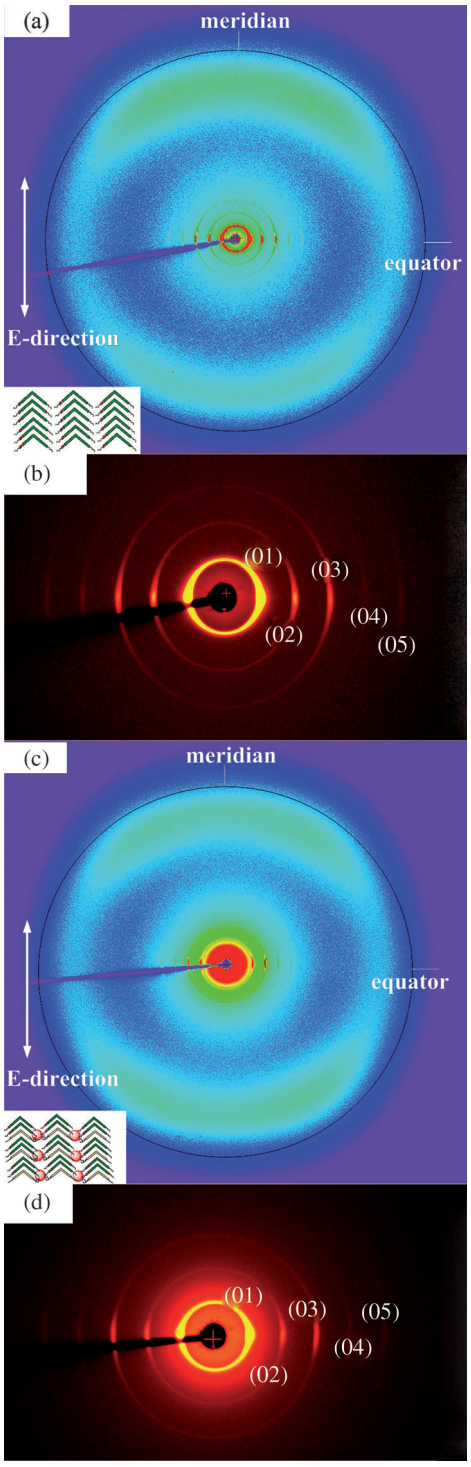

Figure 3. In situ XRD measurements under DC electric fields (200 V, 0.33 $V\,\mu m^{-1}$) of: a) the hydrogen-bonded complex VPy-SiA, b) its expansion in the layer region at 110 °C, c) the nanocomposite VPy-SiA/AuNPs-S (5 wt %; arrangement under a DC electric field of 200 V, 0.33 $V\,\mu m^{-1}$), and d) its expansion in the layer region at 110 °C (arrangement in the absence of an electric field).

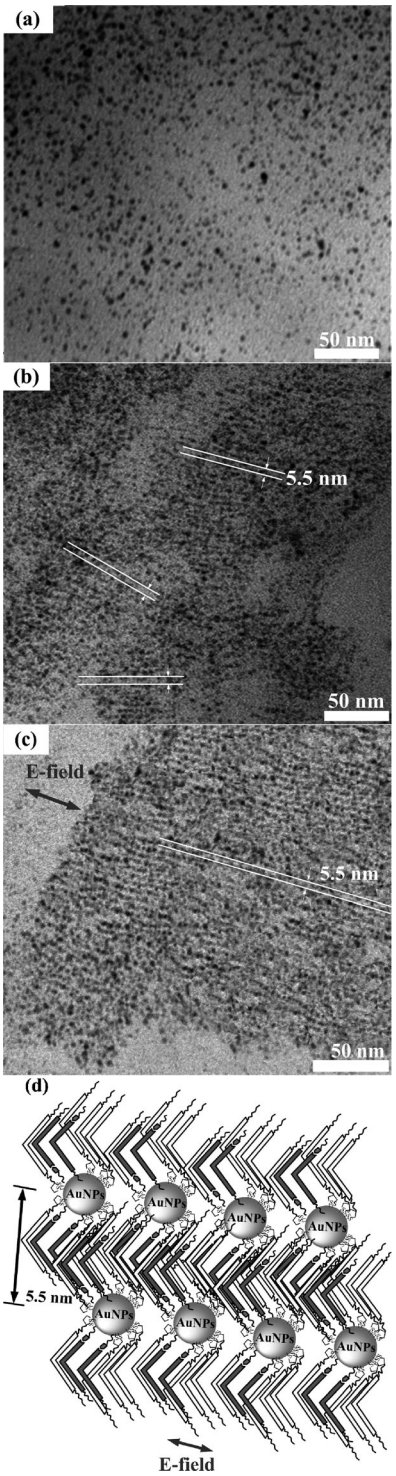

Figure 4. TEM morphologies of the nanocomposite VPy-SiA/AuNPs-S (5 wt%) upon quenching from the LC phase: a) in the absence of a DC electric field, b) under a DC electric field of 200 V (0.33 V μm^{-1}), and c) under an AC electric field of 400 V, $f=1$ Hz (0.66 V μm^{-1}, $f=1$ Hz). d) Cartoon model of the nanocomposite's arrangement under electric fields.

electric field (Figure 4a). As shown in Figure 4b, the TEM image of the nanocomposite VPy-SiA/AuNPs-S (5 wt%) prepared in the presence of a DC electric field revealed that the AuNPs-S was generally aligned into layers (layer spacing: 5.5 nm), in which the slice direction of TEM was parallel to the electric field.

This TEM result perfectly matches the *d* spacing of 5.5 nm obtained through in situ XRD measurements under a DC electric field (Figure 3c). However, curved and distorted directions of the layer structure composed of gold NPs (AuNPs-S; 5 wt%; Figure 4b) would be induced by the turbulent flow of the continuous DC electric field applied between electrodes (0.33 V μm^{-1}). Therefore, to eliminate the effect of the turbulent flow under DC electric fields, the nanocomposite VPy-SiA/AuNPs-S (5 wt%) was further applied by a stronger AC electric field (0.66 V μm^{-1}, 1 Hz) for 1 h to stabilize the layer structure of AuNPs-S in the nanocomposite. Compared with Figure 4b, under a DC electric field, the TEM image of a more ordered and large-scaled layer structure (with a *d* spacing of 5.5 nm) of the nanocomposite VPy-SiA/AuNPs-S (5 wt%) was obtained under an AC electric field (Figure 4c). However, as illustrated in Figure S8 in the Supporting Information, the layer structure in the nanocomposite VPy-SiA/AuNPs-S (1 wt%) with a lower wt% of gold NPs (AuNPs-S) under the same AC electric field (i.e., 0.66 V μm^{-1}, 1 Hz) was not well aligned as that in the nanocomposite VPy-SiA/AuNPs-S (5 wt%). Figure 4d presents a possible cartoon model of the nanocomposite arrangements in the presence of the electric fields. As a consequence, the direct evidence from these TEM images reveals that well-organized packing of surface-modified gold NPs can be induced by the bent-core LC host in the nanocomposite subjected to DC/AC electric fields.

In summary, we have prepared a gold nanocomposite (VPy-SiA/AuNPs-S) incorporating 5 wt% surface-modified gold NPs (AuNPs-S) doped within a hydrogen-bonded bent-core LC complex VPy-SiA. Doping VPy-SiA with an appropriate amount of decorated AuNPs-S led to a broader mesophasic range and lower transition temperatures for the nanocomposite VPy-SiA/AuNPs-S. The altered molecular packing induced by raising the concentration of gold NPs (AuNPs-S) in the SmCP phase resulted in the AF switching behavior of the complex VPy-SiA being changed to the F switching behavior of the nanocomposite VPy-SiA/AuNPs-S (5 wt%). Using our technique for alignment of the bent-core molecules under (DC/AC) electric fields, we could control, in a straightforward manner, the orientations of the molecular stacks (bent-core apexes were aligned along the electric fields) and layer arrangements (layer normals were aligned perpendicular to the electric fields) of the LC molecules (induced by intra- and intermolecular interactions), as confirmed from associated X-ray diffraction patterns. TEM images revealed directly that well-organized packing of layers of surface-modified gold NPs could be induced in the nanocomposite under electric fields, due to the interaction and alignment of the bent-core LC host molecules.

Experimental Section

Synthesis and sample preparation: The detailed synthesis procedures of the receptor monomer (M1) are described in the Supporting Information. The synthesis procedures are shown in Scheme S1–S4 in the Supporting Information. Hydrosilylation of the compounds was mediated by Karstedt's catalyst to provide the corresponding siloxane-substituted materials. All compounds were purified through column chromatography and recrystallization; all synthesis details are described in the Supporting Information. The hydrogen-bonded complex VPy-SiA (bent-core LC host) was prepared by dissolving the hydrogen bond acceptor VPy and the hydrogen bond donor SiA (1:1 molar ratio) in anhydrous THF, evaporating the solvent gradually at 40 °C, and then drying it under vacuum, overnight. By using the same procedure, the hydrogen-bonded nanocomposite VPy-SiA/AuNPs-S was prepared from 1 wt%, 5 wt% of AuNPs-S in the LC host VPy-SiA.

Measurements and characterization: ^{1}H NMR spectra were recorded by using a Varian Unity 300 MHz spectrometer with [D_6]DMSO and CDCl3 as solvents. Mass spectra were recorded by using a Micromass TRIO-2000 GC/MS instrument. Elemental analyses were performed by using a Heraeus CHN-OS RAPID elemental analyzer. Mesophasic textures were characterized by using a Leica DMLP polarizing optical microscope equipped with a hot stage. FTIR spectra were recorded by using a Perkin–Elmer Spectrum 100 spectrometer. A Linkam TSTE350 stage, an MDS 600 and CI 94 controller, and Linksys 32 temperature/motor control software were used as the temperature controlling system. The phase transition temperatures and corresponding enthalpies were determined through differential scanning calorimetry (DSC, model: Perkin–Elmer Pyris 7) under N_2 at heating and cooling rates of 5 °C min^{-1}. Thermogravimetric analysis (TGA) was performed by using a TA-TGA Q-500 instrument (Thermal Analysis) operated at a heating rate of 10 °C min^{-1} under an N_2 atmosphere. TEM was conducted by using JEOL JEM-2011 and Philips Tecnai G2F20 microscopes operated at 200 kV. The samples were cryosectioned by using a Leica Reichert Ultracut E ultramicromote, and the section thicknesses of 30–70 nm were collected on 400-mesh gold grids. In situ electric wide-angle X-ray scattering (WAXS) was performed at an incident wavelength of 1.33 Å by using the BL17A1 beamline of the National Synchrotron Radiation Research Center (NSRRC), Taiwan. The electrodes were composed of stainless steel; the cell gap of the electrodes was 0.6 mm. A Linkam TSTE350 stage, in combination with the previously mentioned temperature controlling system, was used for all WAXS experiments. The electro-optical properties were determined in commercially available indium tin oxide (ITO) cells (Mesostate Corp.; thickness: 7.5 μm; active area: 1 cm^2) with rubbed polyimide alignment coatings (parallel rubbing direction). A digital oscilloscope (Tektronix TDS-3012B) was used in these measurements; a high-power amplifier connected to a function generator (GW: model GFG-813) with a DC power supply (Keithley 2400) was used in the DC field experiments.

Acknowledgements

We thank the financial support from the National Science Council of Taiwan (ROC) through NSC97–2113 M-009-006-MY2.

Keywords: nanocomposites · nanomaterials · nanoparticles · nanostructures · self-assembly

[1] a) T. Teranishi, M. Haga, Y. Shiozawa, M. Miyake, *J. Am. Chem. Soc.* **2000**, *122*, 4237–4238; b) M. C. Daniel, D. Astruc, *Chem. Rev.* **2004**, *104*, 293–346; c) C. J. Kiely, J. Fink, M. Brust, D. Bethell, D. J. Schiffrin, *Nature* **1998**, *396*, 444–446.

[2] a) S. W. Boettcher, N. C. Strandwitz, M. Schierhorn, N. Lock, M. C. Lonergan, G. D. Stucky, *Nat. Mater.* **2007**, *6*, 592–596; b) D. J. Herman, J. E. Goldberger, S. Chao, D. T. Martin S. I. Stupp, *ACS Nano* **2011**, *5*, 565–573.

[3] a) S. W. Lee, C. Mao, C. E. Flynn, A. M. Belcher, *Science* **2002**, *296*, 892–895; b) B. Lindlar, M. Boldt, S. Eiden-Assmann, G. Maret, *Adv. Mater.* **2002**, *14*, 1656–1658.

[4] S. Eustis, M. A. El-Sayed, *Chem. Soc. Rev.* **2006**, *35*, 209–217.

[5] P. N. Prasad, *Nanophotonics*, Wiley, New York, **2004**.

[6] M. Möller, J. P. Spatz, A. Roescher, *Adv. Mater.* **1996**, *8*, 337–340.

[7] a) I. W. Hamley, *Angew. Chem.* **2003**, *115*, 1730–1752; *Angew. Chem. Int. Ed.* **2003**, *42*, 1692–1712; b) J. Y. Chane-Ching, F. Cobo, D. Aubert, H. G. Harvey, M. Airiau, A. Corma, *Chem. Eur. J.* **2005**, *11*, 979–987; c) A. Badia, S. Singh, L. Demers, L. Cuccia, R. Brown, B. Lennox, *Chem. Eur. J.* **1996**, *2*, 359–363; d) G. Shustak, Y. Shaulov, A. J. Domb, D. Mandler, *Chem. Eur. J.* **2007**, *13*, 6402–6407.

[8] a) N. Kimizuka, T. Kunitake, *Adv. Mater.* **1996**, *8*, 89–91.

[9] a) G. P. Mitchell, C. A. Mirkin, R. L. Letsinger, *J. Am. Chem. Soc.* **1999**, *121*, 8122–8123; b) M. Fischler, A. Sologubenko, J. Mayer, G. Clever, G. Burley, J. Gierlich, T. Carell, U. Simon, *Chem. Commun.* **2008**, 169–171.

[10] a) H. Qi, A. Lepp, P. A. Heiney, T. Hegmann, *J. Mater. Chem.* **2007**, *17*, 2139–2144; b) I. In, Y.-W. Jun, Y. J. Kim, S. Y. Kim, *Chem. Commun.* **2005**, 800–801.

[11] a) V. M. Marx, H. Girgis, P. A. Heiney, T. Hegmann, *J. Mater. Chem.* **2008**, *18*, 2983–2994.

[12] a) S. K. Pal Kumar, P. S. Kumar, V. Lakshminarayanan, *Soft Matter* **2007**, *3*, 896–900; b) M. Yamada, Z. Shen, M. Miyake, *Chem. Commun.* **2006**, 2569–2571; c) H. K. Bisoyi, S. Kumar, *Chem. Soc. Rev.* **2011**, *40*, 306–319.

[13] a) J. Y. Lee, J. Lee, Y. J. Jang, J. Lee, Y. H. Jang, S. J. Kochuveedu, C. Park, D. H. Kim, *Chem. Commun.* **2011**, *47*, 1782–1784; b) Q. Dai, D. Berman, K. Virwani, J. Frommer, P. O. Jubert, M. Lam, T. Topuria, W. Imaino, A. Nelson, *Nano Lett.* **2010**, *10*, 3216–3221; c) Y. Kuroda, Y. Yamauchi, K. Kuroda, *Chem. Commun.* **2010**, *46*, 1827–1829.

[14] C. Y. Chao, X. Li, C. K. Ober, C. Osuji, E. L. Thomas, *Adv. Funct. Mater.* **2004**, *14*, 364–370.

[15] O. Francescangeli, V. Stanic, S. I. Torgova, A. Strigazzi, N. Scaramuzza, C. Ferrero, I. P. Dolbnya, T. M. Weiss, R. Berardi, L. Muccioli, S. Orlandi, C. Zannoni, *Adv. Funct. Mater.* **2009**, *19*, 2592–2600.

[16] O. Catanescu, L.-C. Chien, *Adv. Mater.* **2005**, *17*, 305–309.

[17] R. H. Terrill, T. A. Postlethwaite, C. H. Chen, C. D. Poon, A. Terzis, A. Chen, J. E. Hutchison, M. R. Clark, G. Wignall, J. D. Londono, R. Superfine, M. Falvo, C. S. Johnson, E. T. Samulski, R. W. Murray, *J. Am. Chem. Soc.* **1995**, *117*, 12537–12548.

[18] a) W. Hou, M. Dasog, R. W. J. Scott, *Langmuir* **2009**, *25*, 12954–12961; b) L. Cseh, G. H. Mehl, *J. Am. Chem. Soc.* **2006**, *128*, 13376–13377.

[19] a) T. Sekine, T. Niori, M. Sone, J. Watanabe, S. W. Choi, Y. Takanishi, H. Takezoe, *Jpn. J. Appl. Phys.* **1997**, *36*, 6455–6463; b) R. Amaranatha Reddy, B. K. Sadashiva, *Liq. Cryst.* **2003**, *30*, 1031–1050.

[20] C. Keith, G. Dantlgraber, R. A. Reddy, U. Baumeister, C. Tschierske, *Chem. Mater.* **2007**, *19*, 694–710.

Received: July 13, 2011
Published online: October 18, 2011

